ELSEVIER

Applied Surface Science 195 (2002) 175–186

applied surface science

www.elsevier.com/locate/apsusc

Synthesis of selenium nanoparticles by pulsed laser ablation

M. Quintana[a], E. Haro-Poniatowski[a,*], J. Morales[b], N. Batina[b]

[a]*Departamento de Física, Universidad Autónoma Metropolitana Iztapalapa, Apdo. Postal 55-534, Mexico DF 09340, Mexico*

[b]*Departamento de Química, Universidad Autónoma Metropolitana Iztapalapa, Apdo. Postal 55-534, Mexico DF 09340, Mexico*

Received 7 May 2002; received in revised form 7 May 2002; accepted 9 May 2002

Abstract

The synthesis of selenium nanoparticles by pulsed laser ablation using a YAG laser at 532 nm is reported. The nanoparticles were deposited on three different substrates: metallic gold films, silicon wafers and glass, and subsequently visualized and characterized by atomic force microscopy (AFM). It was found that the size, shape and population of the selenium nanoparticles are strongly dependent on the experimental conditions during the ablation process; in particular on the energy density, number of laser pulses and the nature of the substrate. Atomic force microscopy imaging allows recognition, quantitative and qualitative characterization of individual selenium nanoparticles and their aggregates as well. In most of the experiments just a few laser pulses (up to five), were sufficient to produce a noticeable amount of nanoparticles on the substrate surface.

PACS: 81.07; 68.37.P; 81.16.M

Keywords: Nanoparticles; Atomic force microscopy; Pulsed laser deposition

1. Introduction

Nanosized materials have received great attention in the last few years, due to the fact that they have different properties than their corresponding bulk or molecular counterparts. As an example, nanometer sized semiconductor particles have proved to be a very promising material for technological applications, since quantum confinement in such materials modifies the band structure of their bulk counterpart, giving rise to new physical effects [1]. Furthermore, dispersing semiconductor nanoparticles hosted in a transparent material exhibits interesting non-linear optical properties [2]. Although so far several different techniques have been used in order to produce nanosized materials, for operational reasons, the most popular ones are the wet chemical process (co-precipitation, sol–gel and complexation) [3]. Other preparation techniques, involving physical vapor deposition (PVD), like sputtering, vapor phase diffusion and laser ablation (PLD), have distinct advantages over the chemical ones, since these often require a final calcination step, which makes them unsuitable for certain applications. Furthermore, with sputtering and laser ablation the stoichiometry of the material is maintained [4]. With PLD, the size of nanoclusters can be controlled by the laser parameters: power density, wavelength, pulse duration, and by the ambient gas conditions such as

* Corresponding author. Tel.: +52-5804-4610x364; fax: +52-5804-4611.
E-mail address: haro@xanum.uam.mx (E. Haro-Poniatowski).

0169-4332/02/$ – see front matter © 2002 Published by Elsevier Science B.V.
PII: S0169-4332(02)00549-4

pressure, nature of the gas and flow rate. However, as it has been pointed out by Chen [5], depending upon the ablated material, the size of particles is not always uniform and splashing is a common phenomenon in thin film deposition. The characteristics of this nanoparticles also depend on processes occurring at the surface of the substrate, such as nanocluster coalescence and enhanced mobility, which can be controlled by the substrate temperature. Nanosized particles have several interesting features for synthesizing new materials with improved properties compared to the coarser-grained conventional materials. So far the rate of production of such nanomaterials is usually very low. However, the use of laser ablation is expected to give a higher yield [6].

Selenium is a semiconductor and an excellent glass former [7] that has applications in photovoltaic cells and xerography. Furthermore this material exhibits non-linear optical properties such as photo-darkening and optical phase conjugation [5,7–9]. Selenium exists in amorphous (a-Se) and crystalline phases. The main ones being trigonal (t-Se), consisting of helical chains, and monoclinic consisting of Se_8 rings [10]. Amorphous selenium (a-Se) is composed of a mixture of disordered chains [11]. The melting temperature of t-Se is 217 °C [10]. Trigonal Se nanoparticles have been produced by ion implantation into fused silica [12], by colloidal precipitation, capping [13], physical adsorption through vapor phase diffusion [14,15], precipitation and subsequent evaporation of the solvent [7], rf-cosputtering [16], confinement in zeolite pores or cancrinite nanochannels [17–19]. To our knowledge there is no report of the synthesis of a-Se nanoparticles. In the present work, we report on the synthesis and characterization of a-Se nanoparticles by pulsed laser deposition (PLD).

2. Experimental

2.1. Laser ablation setup and sample preparation

The experimental setup for laser ablation of selenium has been described elsewhere [9]. In these experiments, we used the 532 nm harmonic wavelength of a pulsed Nd:YAG laser. Power densities up to 10^8 W/cm^2 with 10 ns pulse were used. The laser beam was focused with a 140 mm focal length spherical lens, with incidence angle of 45°. The spot size at the surface of the target was approximately 2 mm^2. The distance between target and substrate was of the order of 35 mm.

Commercial amorphous selenium (Baker 99.99%) was pressed at 4.8 t/cm^2 to make 5 mm thick and 20 mm in diameter targets. The ablated material was deposited on different substrates: Si(1 0 0) wafers cleaned with acetone, water and HF solution; gold coated glass films with atomically flat Au(1 1 1) terraces, prepared using a procedure previously published [20–22], and glass microscope slides cleaned with ethanol and distilled water. In all cases, the substrate was maintained at room temperature. Target and substrate were placed inside a vacuum chamber with a diffusion pump yielding pressures of 8×10^{-4} Torr. During ablation the target was rotated to avoid depletion of the material at any given spot.

2.2. Atomic force microscopy (AFM) characterization

AFM (Nanoscope III, Digital Instruments, USA) was used for visualization of the selenium nanoparticles deposited on the different substrates. Imaging was performed ex situ, under laboratory atmosphere conditions, operating in the so-called ‘‘tapping’’ mode [23]. In this mode, the AFM tip is oscillating near its resonance frequency and it only touches the sample periodically. This enables minimal sample damaging and provides better images for the sensitive ‘‘soft’’ samples, as is the case for selenium nanoparticles. Imaging was performed using silicon probes (TESP-tips) obtained from digital DI, especially suitable for ‘‘tapping’’ mode imaging. These are in average 4–5 times sharper than those used for the ‘‘contact’’ mode imaging, with cantilevers of 125 μm of length, 30 μm width, 3–5 μm thickness, and a spring constant between 17 and 64 N/m. Typical resonant frequencies between 294 and 375 kHz were used. In each experiment scanning started at 20 μm × 20 μm area, and gradually was reduced to 1 μm × 1 μm. All images were recorded at the very slow scan rate of 1 Hz, in order to avoid sample damaging. Due to these precautions, no impact on the tip or on the sample was observed. Images were recorded in height, amplitude and phase modes simultaneously. As it is well known, the contrast in the height mode imaging is related to

the sample surface topography. Amplitude images show differences between local stiffness and are very useful in composite materials studies. The phase sensitive imaging maps the phase of the cantilever oscillation during the tapping scan, and detects variations in adhesion, friction, visco-elasticity and some other mechanical properties [24–29]. As stated before, monitoring changes in the phase, frequency or amplitude of the AFM response, often leads to data, which are complementary to topography [30]. Images recorded in amplitude and phase modes often have better resolution than those recorded in the height mode, allowing an easier identification and characterization of very small surface objects. In the present study, this was one of the major reasons for using different imaging modes. In order to satisfy the statistic nature of the analysis, five different areas were checked on each sample. However, due to the fact that the ablation system does not allow nanometric positioning, the examined areas are only approximately the same from sample to sample. The presented images show the two-dimensional and three-dimensional mode top-view. Quantitative evaluation of particle size dimension and average film surface roughness (RMS), was performed on the height mode imaging, using the Nanoscope software. The roughness analysis is based on calculation of the standard deviation of all height values within the area under consideration, and expressed as RMS[R_q] (root mean square roughness) factor. For more details, see previous literature on the roughness measurement by AFM [31–35].

2.3. Raman characterization

Raman spectroscopy measurements were performed at room temperature in air with a Spex 1403 double monochromator using the 632.8 nm line of an He–Ne (spectra physics) laser at a power level of 5 mW in a backscattering configuration. The signal was detected with a photomultiplier and a standard photon counting system.

3. Results

In order to determine the best conditions to produce selenium nanoparticles with the pulsed laser deposition system described before, several experiments with different experimental parameters, such as the energy of the laser pulse (the power density), the number of pulses and the substrate type were performed. In a first series of experiments, the effect of the laser power density was investigated maintaining the number of pulses constant. In a second series, the energy density was kept constant and the number of pulses varied. These experiments were performed with a metallic gold substrate, which is very convenient in terms of easy recognition of the nanosized surface features. Deposition on Si wafers and glass substrates yield to a better understanding of diffusion, mobility, and adsorption behavior of Se particles. Before and after selenium deposition all substrates were visualized by atomic force microscopy in order to determine the main surface characteristics of the clean and covered surfaces with Se.

3.1. Selenium deposition on Au(1 1 1) substrates

As explained before, gold film consisting of micron size grains and perfectly flat Au(1 1 1) terraces, were used as substrates in the present study since nanosized features are easily recognizable on their surface. Another advantage is its relatively simple cleaning and maintenance. These aspects make the gold film an ideal surface reference to be used for microscopic analysis.

Fig. 1a and b show AFM images of the clean gold film substrate. Perfectly flat terraces located on the top of huge (micron size) grains can be easily seen in Fig. 1a. The surface texture with numerous grains divided by deep trenches, is better seen on the large image presented in Fig. 1b. Table 1 presents the main gold film surface characteristics as obtained by AFM. Se deposition results in changes in the surface characteristics and morphology, even after deposition by a single laser pulse, as can be observed in Fig. 1c that shows an image (amplitude mode) of the gold substrate recorded after one laser pulse. This picture reveals two types of particles: the large gold grains described before and much smaller Se nanoparticles. The difference is striking enough allowing easy identification of Se nanoparticles based only on size and morphology criteria. The image presented in Fig. 1d shows the gold substrate after being exposed to five laser pulses on the Se target. Characteristics of the

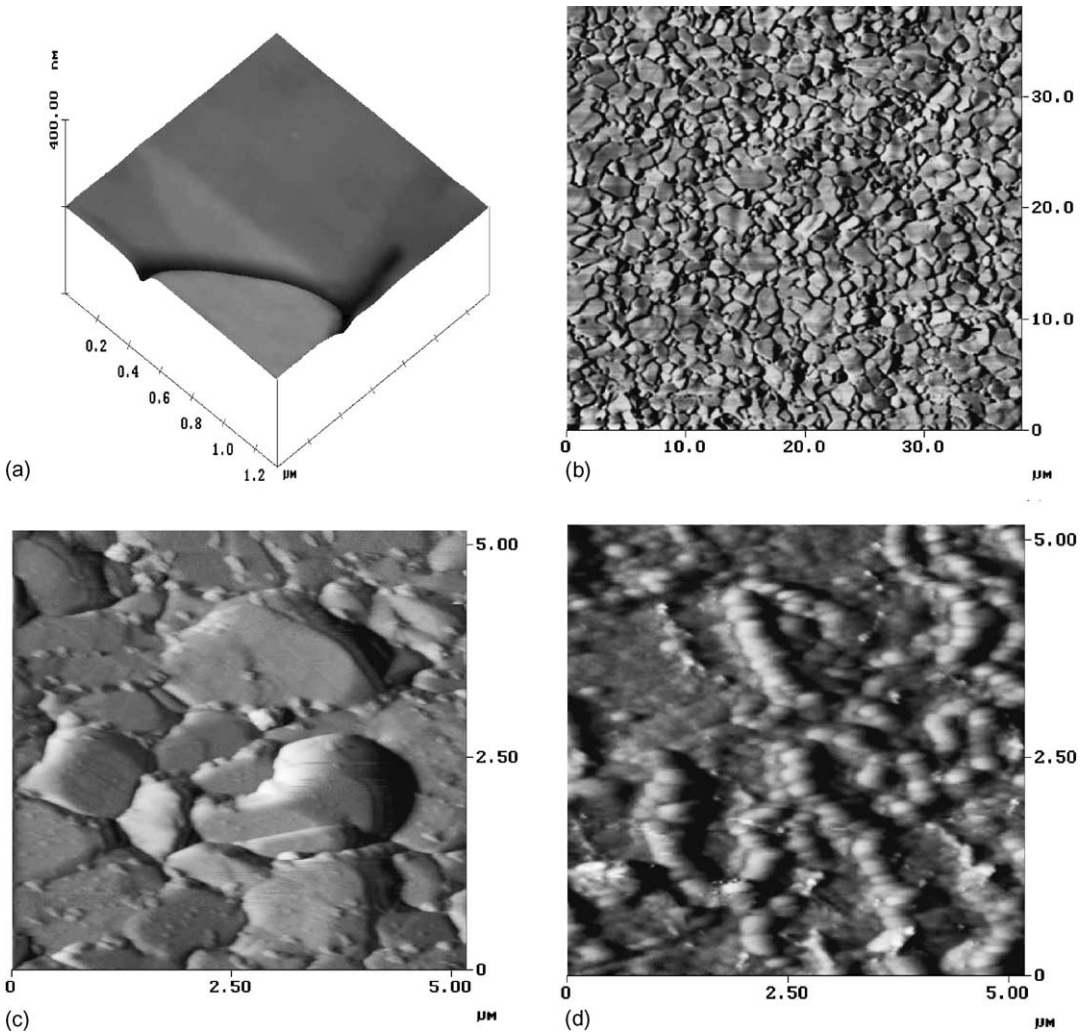

Fig. 1. Tapping mode AFM height (a) and phase image (b), presented as three-dimensional and two-dimensional graphics, respectively, showing the clean gold film substrate, consisting of large grains with atomically flat Au(1 1 1) top surface. Amplitude mode AFM images of the gold film substrate covered by Se nanoparticles after 1 (c), and 5 (d) consecutive laser pulses.

Table 1
Surface characteristics of Au(1 1 1) substrate

System	RMS[R_q] (mm)	Types of grains	Grain diameter (μm)	Grain height (μm)	Distance between grains (μm)
Au(111) substrate	9.00 ± 2.00 (substrate surface)	1	0.5 ± 0.1	30 ± 5	40 ± 20
Au(111) substrate	0.78 ± 0.05 (grain surface)	2	1.5 ± 0.5	30 ± 5	40 ± 20

Data obtained by AFM image analysis.

Table 2
Surface characteristics of Au(1 1 1) substrate with Se deposition and number of laser pulses

System	Number of pulses	Power density ($\times 10^8$ W/cm^2)	RMS[R_q] (nm)	Type of particle	Particle diameter (nm)	Particle height (nm)
Se/Au(1 1 1)	1	10.4	4.75 ± 0.05	Single particle	100 ± 20	3 ± 1
Se/Au(1 1 1)	3	10.4	11.78 ± 0.05	Single particle	75 ± 5	10 ± 4
Se/Au(1 1 1)	5	10.4	6.98 ± 0.05	Aggregates	339 ± 3	14 ± 4

Data obtained by AFM image analysis.

deposited Se particles of both experiments are presented in Table 2. The laser power density in both experiments, 1 and 5 pulses was kept constant at 10.4×10^8 W/cm^2. Comparison of the data presented in Tables 1 and 2, reveals the following trends in surface changes due to deposition after an increase of the number of laser pulses.

As expected, the increase of number of laser pulses led to an increase of the deposited Se material in the substrate. Furthermore, besides single particles, AFM images reveal the existence of aggregated Se particles (larger that 100 nm), seen after 1, 3 and 5 pulses. As seen in the image shown in Fig. 1d, the aggregates preferentially grow along the grain edges of the gold substrate.

Fig. 2a shows the gold film surface when the lowest laser power density available is used for deposition; the analysis of the AFM images reveals that the size of the deposited nanoparticles decreases with a decrease of the laser power density (Fig. 2b). Results are summarized in Table 3. As in the previous case aggregation occurs in the Au grain boundaries. Furthermore, a larger number of single particles, which are dispersed along the surface of the grains in the form of isolated, disk shape, islands are observed. Note that particle diameter is larger than particle height.

3.2. Selenium deposition onto glass substrate

The AFM analysis of Se nanoparticles onto glass substrates presents some difficulties. The surface morphology of the clean glass substrate is very complex as shown in Fig. 3a and data in Table 4. Therefore,

Table 3
Surface characteristics of Au(1 1 1) substrate with Se deposition and laser power density

System	Number of pulses	Power density ($\times 10^8$ W/cm^2)	RMS[R_q] (nm)	Type of particle	Particle diameter (nm)	Particle height (nm)
Se/Au(1 1 1)	1	1.35	–	Single particle	45 ± 20	5 ± 2
Se/Au(1 1 1)	1	2.45	–	Single particle	60 ± 10	15 ± 5
Se/Au(1 1 1)	1	4.25	9.19 ± 0.05	Single particle	100 ± 30	16 ± 1
Se/Au(1 1 1)	1	4.25	9.19 ± 0.05	Aggregates	250 ± 10	20 ± 3
Se/Au(1 1 1)	1	10.4	4.75 ± 0.05	Single particle	110 ± 10	3 ± 1

Table 4
Results of the AFM analysis of the glass sample before and after Se deposition

System	Number of pulses	Power density ($\times 10^8$ W/cm^2)	RMS[R_q] (nm)	Type of particle	Particle density (%)	Particle diameter (nm)	Particle height (nm)
Glass substrate (optical microscope slide)	–	–	2.64 ± 0.05	Single particle	82	125 ± 25	9.5 ± 0.5
			2.64 ± 0.05	Aggregates	15	300 ± 10	25 ± 2
Se on the glass substrate	20	18.9	5.49 ± 0.05	Single particle (1)	80	90 ± 10	8 ± 1
			5.49 ± 0.05	Single particle (2)	20	294 ± 56	45 ± 2

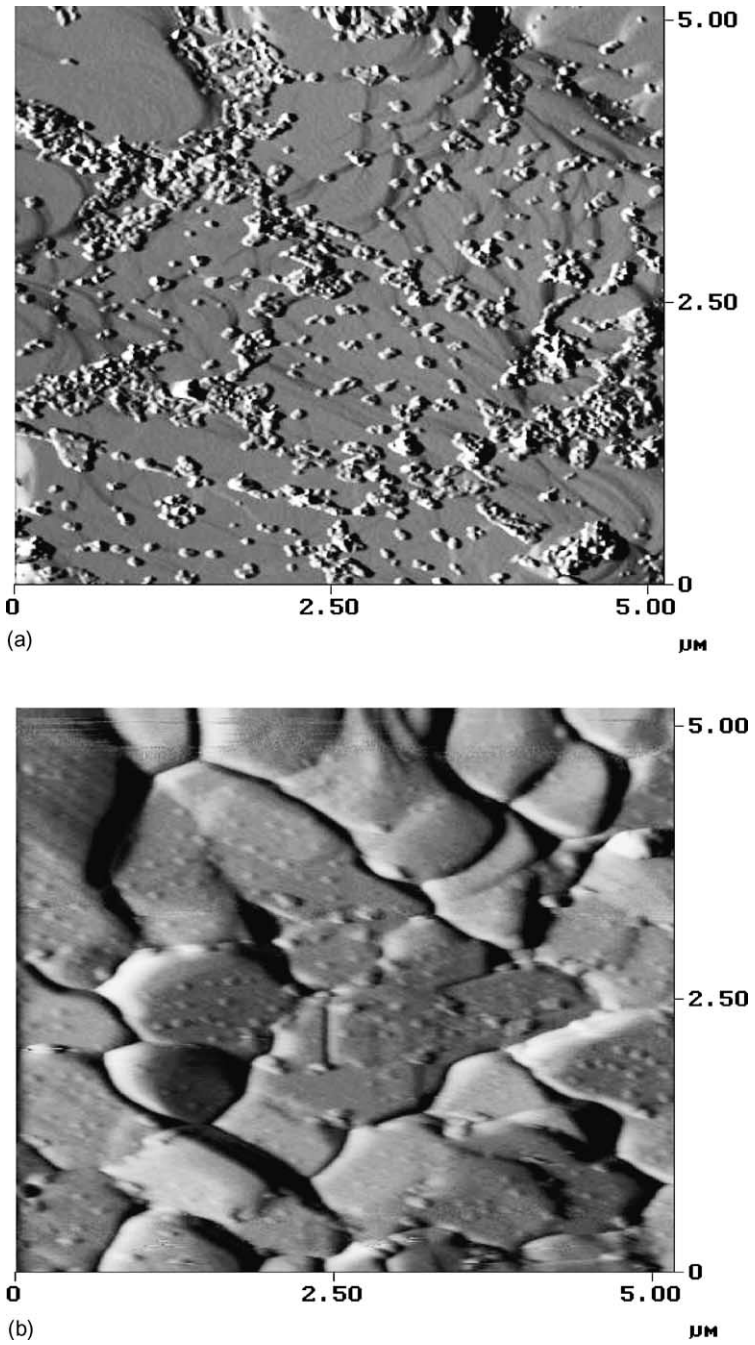

Fig. 2. AFM images show difference in distribution of Se nanoparticles at the gold film substrate (large grains) after the first laser pulse of two different energy densities: 1.35×10^8 W/cm^2 (a), and 10.4×10^8 W/cm^2 (b). Images were recorded in the amplitude mode.

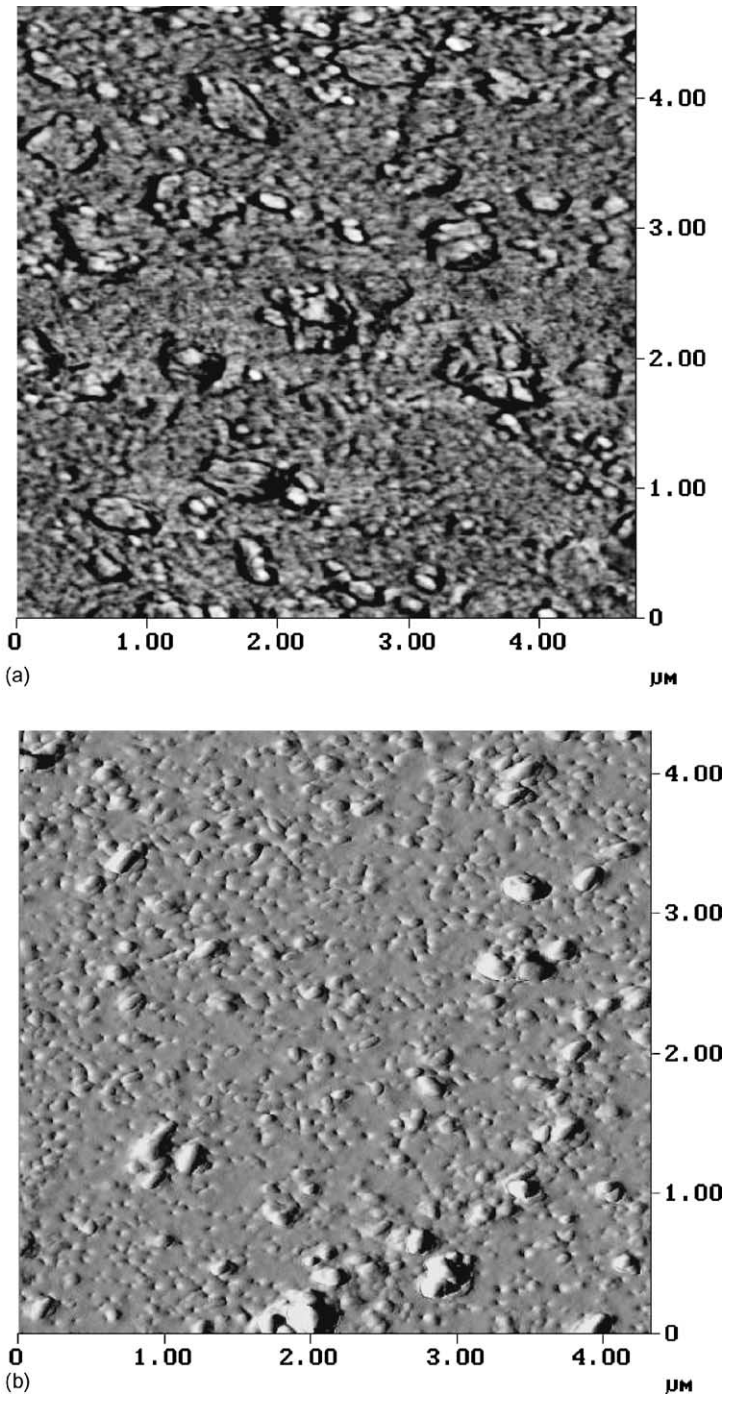

Fig. 3. AFM images of the glass substrate before (a), and after (b) 20 laser pulses. Images were recorded in phase and amplitude modes, respectively.

identification of deposited nanoparticles was difficult, particularly from images recorded in the height mode (topography). Phase imaging, reflecting the mechanical properties and images recorded in the amplitude mode (local stiffness) were more useful, allowing to observe clear edges of the nanofeatures. However, one could not say that single, individual Se nanoparticles were identified successfully. Fig. 3a and b. show tapping mode AFM images of glass substrate free (a) and covered by a film of Se nanoparticles (b). This sample was obtained by laser ablation with 20 pulses. Images were recorded in phase mode (a), and amplitude mode (b). Results of a quantitative evaluation of the AFM images are presented in Table 4. It is surprising that there are no striking differences between surface features for clean and selenium covered glass substrates. It seems that even particle size (diameter of the visualized features) of the deposited material and the substrate are very similar. Taking all these results into account, as well as the visual information from the images in Fig. 3a and b, we suppose that Se essentially grows smoothly on the surface of the glass substrate and forms a film whose topographical characteristics are very close to those of the substrate. This is also confirmed by the rather small change of the RMS[R_q] factor which is an average of the surface roughness value (from 2.64 to 5.49 nm). Assuming that surface roughness is a function of the film particle size, this indicates that particles on both surfaces (free and covered) are very similar.

3.3. Selenium deposition on Si(1 0 0) wafers

Fig. 4a–c, show AFM images of Se nanoparticles deposited on the Si-wafer (1 0 0) surface. Images a and b are presented as three-dimensional graphics clearly emphasizing the topographic characteristics of the imaged area. Both images of the Si-wafer were recorded in the height mode, after being exposed to 1 (Fig. 4a) and 10 (Fig. 4b) pulses. On both images single isolated Se nanoparticles can be clearly seen. With one pulse, only few nanoparticles, preferentially deposited at surface defects, were found. After 10 pulses, the deposited particles were found all over the substrate, but still in the form of single clusters, with no sign of any associative processes. Table 5 shows the quantitative analysis of the surface characteristics for

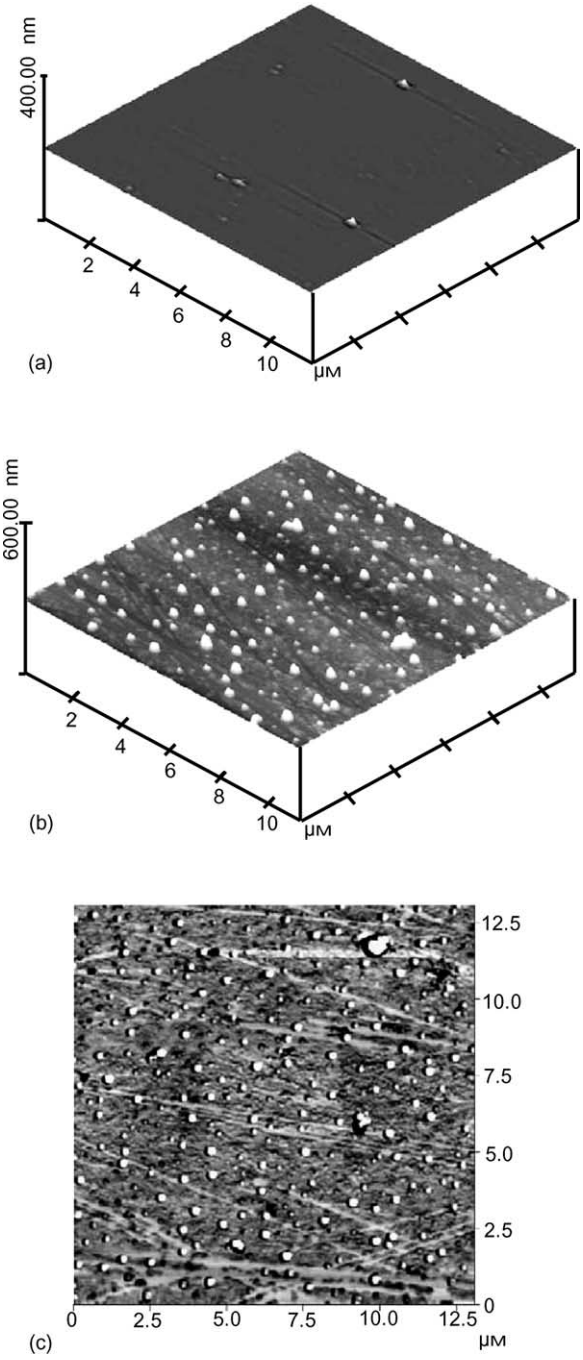

Fig. 4. Surface topography of the Si(1 0 0) substrate populated by Se nanoparticles as a function of the number of the laser pulses: 1 pulse (a), and 10 pulses (b), respectively. The phase image (c) of (b) clearly emphasizes the shape and position of the Se nanoparticles on the silicon-wafer surface.

Table 5
Surface characteristics of the Si-wafer sample covered by Se nanoparticles

System	Number of pulses	Power density ($\times 10^8$ W/cm^2)	RMS[R_q] (nm)	Type of particle	Particle density (particle per 100 square microns)	Particle diameter (nm)	Particle height (nm)
Se on Si-wafer	1	10.4	0.27 ± 0.05	Single particle	~5	360 ± 90	7.5 ± 4.5
Se on Si-wafer	10	10.4	4 ± 0.05	Single particle	105 ± 10	300 ± 100	3 ± 1
						300 ± 100	20 ± 10

Se deposited on Si-wafer. Although no analysis was made on clean Si, it is obvious that the increase in the number of laser pulses results in more Se material deposited on the substrate. The few nanoparticles found after one pulse are large but with small height. Note that if the scale in these images were the same, the observed features would look like flat discs (coin-shape islands). In the case of 10 pulses two types of characteristic nanoparticles can be recognized, only differentiated by height.

Fig. 4c shows an AFM phase image of the same area as the one in Fig. 4b and demonstrates how phase imaging can be useful for better detection of the nanoparticle material. Namely, as can be seen in this image, Se nanoparticles have a different contrast than the rest of the surface and are clearly distinguishable. This image also allows determining location of the nanoparticles on the substrate surface.

3.4. Raman spectroscopy measurements

An important issue is whether Se nanoparticles are amorphous or crystalline, specially considering that the gold substrates have a (1 1 1) crystalline orientation. Direct evidence by AFM could not be obtained, however, considering previous work [9], we assume that Se particles are amorphous. In order to verify this hypothesis, we have grown a thick film of selenium using 10 000 pulses and investigated the structure by Raman spectroscopy. The obtained Raman spectrum is presented in Fig. 5, and it clearly shows that the deposited material is, at least, partially amorphous.

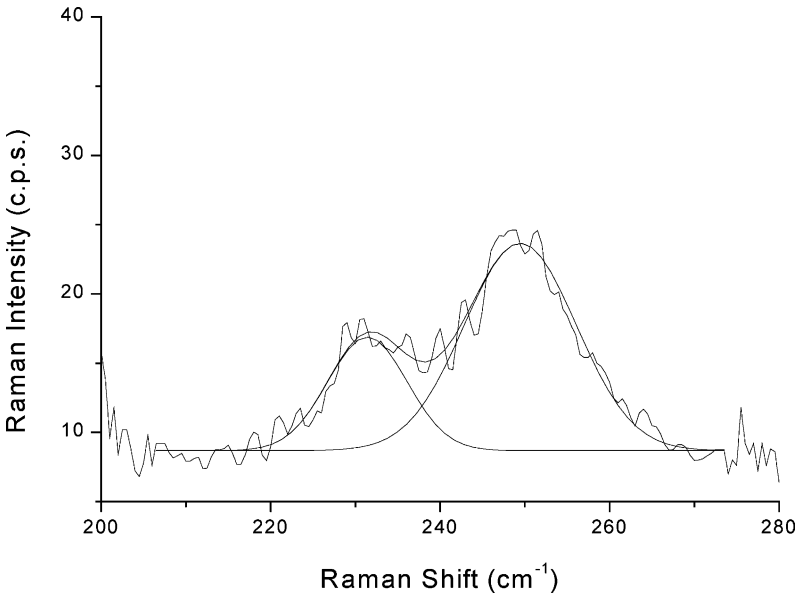

Fig. 5. Raman spectra of Se thin film on glass produced by PLD after 10 000 pulses.

The band at 250 cm^{-1} corresponds to the A_1 mode of amorphous selenium [11,18,36]. The weaker band at 233 cm^{-1} is an indication that crystallization has occurred produced by laser heating during the collection of the Raman spectra [15]. Further attempts to visualize the structure of the Se nanoparticles by AFM on the Au(1 1 1) substrate are under progress.

4. Discussion

One of the goals in this work is to correlate the number of nanoparticles seen in AFM images with the number of laser pulses. In general, we saw that number of nanoparticles increases with the number of pulses. However, this relation is not straightforward, due to two major reasons. On the first place, as mentioned before, each experiment was performed on different samples and different areas were scanned. On the second place, the density of the deposited selenium particles is not uniform within the same sample. It is well known that deposited films obtained by PLD method are not homogeneous in thickness, i.e. the films are thicker in front of the center of the plume. Therefore, a higher population of nanoparticles at this particular position is expected [38].

The present results are only indicative in this particular aspect, however, further experiments are in progress to obtain more quantitative results. In order to minimize such effect, we always try to take images and evaluate deposit around the physical center of the sample.

4.1. Se/Au

An interesting result of our study is that even a single pulse is sufficient to produce a noticeable amount of Se nanoparticles deposit, which is located mainly around the substrate grains, after particle migration along the substrate surface. Furthermore, an increase in the laser power density results in larger particles and aggregation.

Fig. 6 shows the diameter size and particle height as a function of the applied energy density. The increase in particle diameter (open circles) is higher than the increase in particle height (full circles). Furthermore, it is observed that the diameter of the nanoparticle reaches a asymptotic value as a function of the laser power density (w). This suggests that growth is occurring two dimensionally by spreading along the surface in the form of isolated islands having disc shape. Moreover, aggregates have the same height as

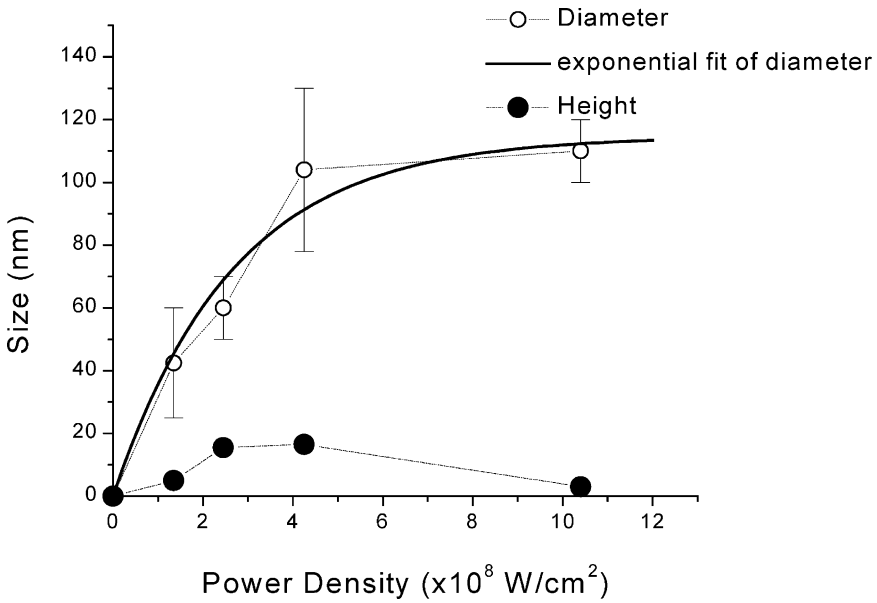

Fig. 6. Diameter (open circles) and height (full circles) of Se nanoparticles as function of the laser power density (1 pulse).

individual particles supporting the assumption of a two-dimensional growth. The continuous line in Fig. 6 represents a simple data adjustment using the equation:

$$D = D_0(1 - e^{-bw})$$

where D is the diameter of the particle and D_0 is its maximum diameter, which is found to be around 114 nm. It is well known that the amount of target material removed increases with the laser power density [38]. However, this does not necessarily means that clusters can grow indefinitely: there is a free energy barrier for nucleation given by the several interface energies (vapor-surface, vapor-cluster and surface-vapor energies) and the change in volume free energy on condensation of the cluster [37], which limits the growth of single particles. These considerations have to be taken into account in order to determine the physical meaning of constant b. Additional experiments need to be performed to elucidate this point.

4.2. Se/glass

In this system, Se did not form aggregates even after 20 laser pulses, which indicates that Se–Se interaction is weaker than Se–substrate (glass) interactions. In this case, the energetic particles of the plume arriving to the glass substrates produce defects on its surface, due to nuclear stopping, and make the tetrahedral network structure of the glass to be displaced from the equilibrium positions to the extent that Si–O dangling bonds are formed [12]. Therefore, it is energetically favored for the arriving Se species to spread uniformly in the substrate surface, and not to form isolated aggregates, as it is shown by the rather small RMS increase after 20 pulses. This is one of the first evidence in our study about significance and difference between substrates. Certainly, the behavior of Se deposit on the gold (metallic) substrate is completely different. When a thin film is already formed on the glass substrate, Se particles grow on three dimensions, with the consequence of a somewhat higher RMS[R_q] factor (from 2.64 to 5.49 nm). In gold instead, less number of pulses, even one pulse, is enough to change the surface morphology.

4.3. Se/Si

As in the case of the gold substrate, the isolated nature of the Se particles on the Si surface suggests that interactions between the Se nanoparticles are weaker than the Se–substrate interaction, so newly deposited material prefers to form its own cluster rather than joining pre-existing structures. This is also supported by the fact that the size of the Se particles after a 10 pulses deposition is similar to the one pulse deposition experiment. The flat disc shape of the Se nanoparticles suggests that they grow as two-dimensional objects (lateral spreading) and that the growth mechanism is probably of progressive type. According to the AFM image analysis, the increase of number of pulses by 10 times results in an increase of the surface roughness (RMS[R_q] factor) of almost 15 times. This may be due to an increase of the nanoparticle density.

In the case of crystalline substrates, in a first stage, light Se species from the plume, with the highest kinetic energy, will be responsible for the formation of island monolayers, forming nucleation centers. When Se particles arrive to the substrate—formed during the plume expansion—diffusion mechanisms will make them to attach either to lower energy zones of the substrate (Au grain boundaries, e.g.) or to the first island monolayers, depending on Se–Se species or Se–substrate bonding energies.

The above results show a clear substrate dependence of the morphology, distribution and characteristics of the deposited material. Although particles grow preferentially in two-dimensional objects on all substrates, it seems that a growth mechanism of the type of the Stransky–Krastanov mechanism [37] is responsible for the Se particle growth in the deposition experiments on Si wafers. A highly crystalline substrate surface yields to a higher diffusion coefficient as seen in the lower area of a-Se deposition shown in Au and Si substrates as it is compared with the glass case.

5. Conclusions

In this work, the synthesis by PLD and characterization of selenium nanoparticles by AFM is presented. Three types of substrates were used, Au(1 1 1) thin films, glass and Si(1 0 0) wafers. The morphology of the particles strongly depends on the substrate. In general, the size and population of particles increases with the laser energy density used for the deposition. In contrast to the Au and Si substrates, where the Se nanoparticles form granular-like structures, in glass

substrates Se spreads tending to cover larger areas uniformly. The obtained results clearly show that PLD is a promising and very useful method for controlled nanoparticle growth. Furthermore, AFM is a suitable tool for nanoparticle characterization.

Acknowledgements

The authors acknowledge financial assistance from CONACYT-Mexico, through research projects 4225-E9405 (E.H.P.-) and L0081-E9608 (N.B.) and the Instituto Mexicano del Petroleo-IMP, through research project: FIES-98-100-I. M.Q. acknowledges CONACYT-Mexico for scholarship support.

References

[1] W.L. Wilsen, P.F. Swajowski, L.E. Brus, Science 262 (1993) 1242.
[2] J.M. Ballesteros, R. Serna, J. Solís, C.N. Alfonso, A.K. Petford-Long, D.H. Osborne, R.F. Haglund Jr., Appl. Phys. Lett. 71 (1997) 2445.
[3] M.L. Hitchman, K.F. Jensen (Eds.), Chemical Vapor deposition: Principles and Aplications, Academic Press, New York, 1997.
[4] R.K. Singh, J. Narayan. Phys. Rev. B 41 (1990) 8843.
[5] L.C. Chen, in: D.B. Chrisey, G.K. Hubler (Eds.), Pulsed Laser Deposition of Thin Films, Wiley, New York, 1994, p. 195.
[6] A. Kar, J. Mazumder, Phys. Rev. E 49 (1994) 410.
[7] M. Rajalakshmi, A.K. Arora, Solid State Commun. 110 (1999) 75–80.
[8] W. Marine, L. patrone, B. Luk'yanchuk, M. Sentis, Appl. Surf. Sci. 154/155 (2000) 345–352.
[9] M. Fernández Guasti, L. Ponce, E. Haro Poniatowski, E. Jímenez, R. Diamant, J. Mater. Sci. 30 (1995) 6253.
[10] W.C. Cooper, R.A. Westbury, in: R.A. Zhingaro, W.C. Cooper (Eds.), Selenium, Van Nostrand Reinhold, New York, 1974, p. 16.
[11] S. Kohara, A. Goldbach, N. Koura, M.-L. Saboungi, L.A. Curtiss, Chem. Phys. Lett. 287 (1998) 282.
[12] D.O. Henderson, M. Wu, A. Ueda, Y.S. Tung, R. Mu, J. Chen, Z. Gu, W.E. Collins, C.W. White, J. Budai, A. Meldrum, R.A. Zuhr, J.G. Zhu, Nucl. Instrum. Meth. Phys. Res. 141 (1998) 284.
[13] A. Peled, V. Baranauskas, C. Rodrigues, D. Art-Weisman, L. Grantmany, A.A. Friesem, J. Appl. Phys. 77 (1995) 6208.
[14] Zi Kang Tang, Michael M.T. Loy, T. Goto, J. Chen, R. Xu, Solid State Commun. 101 (1997) 333.
[15] V.V. Poborchii, A.V. Kolobov, J. Caro, V.V. Zhuravlev, K. Tanaka, Chem. Phys. Lett. 280 (1997) 17.
[16] Y. Maeda, N. Tsukamoto, Y. Yazawa, Y. Kanemitsu, Y. Masumoto, Appl. Phys. Lett. 59 (1991) 3168.
[17] A.V. Kolobov, H. Oyanagi, V.V. Poborchii, K. Tanaka, Phys. Rev. B 59 (1999) 9035.
[18] A. L Goldblach, L.E. Iton, M.-L. Saboungi, Chem. Phys. Lett. 281 (1997) 69.
[19] A.V.V. Poborchii, in: H. Chon, S.K. Ihm, Y.S. Uh (Eds.), Progress in Zeolite and Microporous Materials Studies in Surface Science and Catalysis, Elsevier, Amsterdam, 1997, p. 631.
[20] N. Batina, T. Will, D.M. Kolb, Disc. Faraday Soc. (1992) 94.
[21] D.M. Kolb, A.S. Dakouri, N. Batina, in: A.A. Gewirth, H. Siegenthaler (Eds.), Nanoscale Probes of the Solid/Liquid Interface, Vol. E288, NATO ASI Series C, Sophia Antipolis, Kluwer Academic Publishers, Dordrecht, 1995, p. 1.
[22] T. Will, M. Dietterle, D.M. Kolb, in: A.A. Gewirth, H. Siegenthaler (Eds.), Nanoscale Probes of the Solid/Liquid Interface, Vol. E288, NATO ASI Series C, Sophia Antipolis, Kluwer Academic Publishers, Dordrecht, 1995, p. 37.
[23] S.N. Maganov, M.H. Ahangbo, Surface Analysis with STM and AFM, VCH, Weinheim, 1994.
[24] A.G. Gilicinski, C.R. Hegedus, in: T. Proder, M. Winnik, M. Urban (Eds.), Film Formation in Waterborne Coatings, 1996, p. 286.
[25] R. Brandsch, G. Bar, M.-H. Whangbo, Langmuir 13 (1997) 6349.
[26] S.N. Maganov, V. Elings, V.W. Papkov, Polymer 38 (1997) 297.
[27] X. Chen, M.C. Davies, C.J. Roberts, S.J.B. Tendler, P.M. Williams, J. Davies, A.C. Dawkes, J.C. Edwards, Ultramicroscopy 75 (1998) 171.
[28] A. Omiake, G. Chen, G.W. Van Loon, J.H. Horton, Langmuir 14 (1998) 4731.
[29] D. Raghavan, M. Van Landingham, X. Gu, T. Nguyen, Langmuir 16 (2000) 9448.
[30] C. Schellenberg, S. Akari, M. Regenbrecht, K. Tauer, F.M. Petrat, M. Antonietti, Langmuir 15 (1999) 1283.
[31] M.T. McDermott, C.A. McDermott, R.L. McCreery, Anal. Chem. 65 (1993) 937.
[32] R.J. Phillips, T.D. Golden, M.D. Shumsky, J.A. Switzer, J. Electrochem. Soc. 141 (1994) 2391.
[33] D. Aubach, Y. Cohen, J. Electrochem. Soc. 143 (1996) 3525.
[34] Y.G. Li, A. Lasia, J. Appl. Electrochem. 27 (1997) 643.
[35] E. Sosa, G. Carreño, C. Ponce-de-León, M.T. Oropeza, M. Morales, I. González, N. Batina, Appl. Surf. Sci. 153 (2000) 245.
[36] V. Poborchii, A. Kolobov, T. Kazonubu, Appl. Phys. Lett. 72 (1998) 1167.
[37] J.S. Horowitz, J.A. Sprague, in: D.B. Chrisey, G.K. Hubler (Eds.), Pulsed Laser Deposition of Thin Films, Wiley, New York, 1994, p. 229.
[38] K.L Saenger, in: D.B. Chrisey, G.K. Hubler (Eds.), Pulsed Laser Deposition of Thin Films, Wiley, New York, 1994, p. 199